

Magnetic and Magnetoresistance Behaviors of Particulate Iron/Vinyl Ester Resin Nanocomposites

Zhanhu Guo* and H. Thomas Hahn

*Mechanical & Aerospace Engineering Department and Materials Science & Engineering Department,
University of California, Los Angeles, California 90095, USA*

Hongfei Lin

Department of Chemical Engineering, University of California, Santa Barbara, California 93106, USA

Amar B. Karki and David P. Young

Department of Physics and Astronomy, Louisiana State University, Baton Rouge, Louisiana 7080, USA

Magnetoresistance (MR) behavior of vinyl ester monomer stabilized iron nanoparticles and heat-treated vinyl ester resin nanocomposites reinforced with iron nanoparticles were investigated. Vinyl ester monomer serves as a coupling agent with one side covalently bound onto the nanoparticle surface by a displacement reaction and the other end copolymerized with extra vinyl ester resin to form a robust unity. The spacer distance (particle loading) and materials (polymer or carbonized polymer) have a significant effect on the magnetic and MR properties. The heat-treated nanocomposites follow a tunneling conduction. By simply annealing in a reducing environment, the obtained nanocomposites possess a room temperature MR of 8.3 % at a field of 90 kOe.

* Electronic mail: nanomaterials2000@gmail.com

I. INTRODUCTION

Polymer nanocomposites with functional particles have spurred much interest due to their light weight and cost-effective processability. Inorganic nanofillers dispersed in a polymer matrix can stiffen and strengthen the nanocomposites,¹ increase the electric and thermal conductivities,²⁻⁴ introduce unique physicochemical properties such as magnetic⁵ and optical properties,⁶⁻⁸ and even improve the shape replicability.⁹ As a result, many applications become feasible, such as microwave absorbers,¹⁰⁻¹² photovoltaic (solar) cells,¹³ and smart structures.^{14,15} Metallic multilayer giant magnetoresistance (GMR) has found wide applications in areas such as biological detection,¹⁶ magnetic recording and storage systems,¹⁷ and rotational sensors in automotive systems¹⁸ since the discovery of GMR in 1988.¹⁹

Compared with the metal-based multilayer GMR sensors, the polymer nanocomposite-based sensors would have the benefit of easy manipulation and cost-effective fabrication. However, the challenge is to obtain high-quality polymer nanocomposites with nanoparticles uniformly dispersed in the polymer matrix. In other words, to prevent particle agglomeration is an inherent challenge in the composite fabrication.²⁰ In addition, the interaction between the nanoparticles and the polymer matrix plays an important role in the quality of the nanocomposite. Poor linkage, such as the presence of gas voids will result in deleterious effects on the mechanical properties of the nanocomposites.^{21,22} Different methods have been developed to prepare polymer nanocomposites with improved particle dispersion quality and enhanced particle-polymer interfacial interaction. Recently, we reported a room temperature GMR of 7.3 % at 90 kOe

in heat-treated iron nanoparticles reinforced polyurethane nanocomposites fabricated by a surface initiated polymerization (SIP) method.²³ In this paper, we report on the fabrication and characterization of a granular GMR nanocomposite that consists of iron nanoparticles dispersed in a vinyl ester resin matrix. The subsequent annealing effect on the magnetic and transport properties is also reported.

II. EXPERIMENT

The processing starts with the fabrication of a cured vinyl ester resin composite reinforced with Fe nanoparticles having an approximate diameter of 20 nm (provided by QuantumSphere Inc.). The bare iron nanoparticles are very reactive and get oxidized very easily. The core-shell structures in the bright-field transmission electron microscope (TEM) image shown in the inset of Figure 1 indicate partial oxidation of the particles arising from TEM sample preparation. The nanoparticle production, transportation and composite fabrication are all done in an ultra-high purity nitrogen atmosphere to prevent particle oxidation.

The nanocomposite fabrication is briefly described as follows. A specific amount of iron nanoparticles in a 2-neck flask are wetted by the nitrogen-degassed vinyl ester resin (30 g) under ultrasonically stirred conditions and mixed for another 2 hours until uniform dispersion is obtained. A mixture of the nitrogen-degassed catalyst (2.0 wt%, Trigonox 239-A, organic peroxide, Akzo Nobel Chemicals) and promoter (0.3 wt%, cobalt naphthenate, OM Group, Inc.) is introduced quickly. The final solution is poured into silicone molds for 24-hour room temperature curing followed by a two-hour postcuring at

100 °C. Vinyl ester resin in the nanocomposites was found to be fully cured under differential scanning calorimetry (DSC) measurement.

Nanocomposites with different particle loadings were fabricated based on the functionality of the vinyl ester monomers and the surface chemistry of the nanoparticles. The hydroxyl groups of the vinyl ester monomers displace with the iron nanoparticles as verified by x-ray photoelectron spectroscopic and FT-IR spectroscopic studies. The carbon-carbon double bonds on the other side of the vinyl ester monomers form a cross-linking with the extra vinyl ester resin (styrene for polymer chain growth or vinyl ester monomers for polymer cross-linking growth) for robust nanocomposite formation. In order to carbonize the matrix, the nanocomposites with different particle loadings were heat treated at 450 °C for 2 hours in hydrogen gas, balanced with ultra-high purity argon (5%). Particle structures were characterized on a FEI Tecnai G2 Sphera transmission electron microscope (TEM) with an accelerating voltage of 200 kV. Weight percentage of nanoparticles in the nanocomposites was determined by thermogravimetric analysis (TGA, PerkinElmer) with an argon flow rate of 50 cm³/min. The polymer matrix, particle loading and heat treatment effect on the magnetic properties were investigated in a 9-Tesla Physical Properties Measurement System (PPMS) by Quantum Design. The electric conductivity and magnetic field dependent resistance were carried out using a standard four-probe method.

III. RESULTS AND DISCUSSION

Figure 1 shows the room-temperature hysteresis loops of the as-prepared and heat-treated vinyl ester monomer stabilized iron nanoparticles. The samples were prepared by a

displacement reaction between iron nanoparticles and the vinyl ester resin in ultrasonication and nitrogen protection conditions. The mixture was washed with tetrahydrofuran and dried in a vacuum oven at room temperature. As compared to the reported coercive force (coercivity, H_c) of 5 Oe for the bare superparamagnetic iron nanoparticles, coercivity is observed to increase to 153 Oe after stabilization with vinyl ester monomers. This is due to the interparticle dipolar interaction within the nanocomposite with a uniform dispersion of single-domain nanoparticles, consistent with a particle-loading dependent coercivity in the nanoparticle assembly.²⁴ Little coercivity difference is observed in the samples after annealing. However, the saturation magnetization (M_s , 76 emu/g) of the as-prepared nanocomposites increases to 109 emu/g after the heat treatment, due to the decomposition of vinyl ester monomers. The lower saturation magnetization in both composite samples indicates that the majority of the iron atoms on the nanoparticle surface have become a nonmagnetic salt by the displacement reaction.

The as-prepared vinyl ester monomer stabilized Fe nanoparticles exhibit lower electric resistivity as compared to the one after heat treatment as shown in Figure 2(a). The resistivity of the monomer stabilized iron nanoparticles increases slowly with decreasing temperature in the range of room-temperature to 100 °C and then remains constant at temperatures lower than 100 °C. However, the nanocomposites become less conductive after the heat treatment. The resistivity increases slowly from room-temperature to 100 °C and suddenly increases beyond the equipment limitation. The linear relation between logarithmic resistivity and the square root of temperature $T^{-1/2}$ shown in Figure 2(b)

indicates a tunneling conductive mechanism for the heat-treated vinyl ester monomer stabilized nanoparticles. Both non-metallic behaviors were observed in the as-prepared and heat-treated monomer stabilized iron nanoparticle samples, indicating that vinyl ester monomers and the subsequently carbonized vinyl ester have effectively protected Fe nanoparticles from oxidation. However, there are three regions for the as-prepared vinyl ester monomer stabilized nanoparticles as shown in Figure 2(b). This behavior could be due to the thermal shrinkage/expansion of the stabilized polymer chain with a change of the temperature.

MR (%) in the composite is defined as:

$$MR(\%) = \frac{R(H) - R(0)}{R(0)} \times 100$$

where $R(H)$ and $R(0)$ are the resistivity at a field of H and zero, respectively. A room temperature GMR of 1.7% is observed in the heat-treated vinyl ester monomer stabilized iron nanoparticles as shown in inset of Figure 2(b). However, only 0.9% MR is observed in the as-prepared vinyl ester monomer stabilized iron nanoparticles.

The particle distribution within the cured vinyl ester resin matrix before the heat treatment was characterized by a scanning electron microscope (SEM). The polymer nanocomposite samples with a particle loading of 40 wt% were prepared by polishing the cured vinyl ester resin samples with 4000 grit sandpaper. The inset of Figure 3(a) shows the typical SEM images of the cross-section of the nanocomposite. The uniform particle dispersion within the polymer matrix indicates that vinyl ester resin has effectively protected the iron nanoparticles from agglomeration. Further X-ray photoelectron

spectroscopy (XPS) investigation indicates a strong particle-polymer interaction through the displacement reaction between the reactive nanoparticles and the vinyl ester resin monomers.

A large shrinkage is observed in the nanocomposites after a two-hour annealing at 450 °C. There is no further polymer residue observed after the heat-treatment as evidenced by FT-IR investigation. These results indicate a complete decomposition of the cured vinyl ester resin in the polymer nanocomposites. Figure 3(b) shows the TEM bright field microstructures of the nanocomposite (40 wt%) after heat treatment at 450 °C for 2 h. The left inset of Figure 3(b) shows the selected area electron diffraction (SAED) patterns of the annealed polymer nanocomposites. The inner ring of the SAED patterns with a d-spacing of 0.34 nm clearly indicates the formation of graphite carbon.²⁵ The obvious core-shell structure arises from the atomic number difference between iron and carbon. The right inset of Figure 3(b) shows the high-resolution TEM microstructure of the annealed polymer nanocomposites. The observed clear lattice fringes indicate the formation of highly crystalline nanoparticles and the calculated lattice distance of 0.205 nm corresponds to Fe.

Figure 3(a) shows the room-temperature hysteresis loops of the vinyl ester resin nanocomposites with a particle loading of 15 and 40 wt% before and after heat-treatment, respectively. Larger coercivity (230 Oe) is observed after the Fe nanoparticles are dispersed in the vinyl ester resin nanocomposites, as compared to those of the bare superparamagnetic iron nanoparticles and vinyl ester monomer stabilized iron nanoparticles. This indicates a weak interparticle dipolar interaction after the nanoparticles

are dispersed into the polymer matrix. However, H_c is much lower than those (685 and 900 Oe for 65 and 35 wt% loading, respectively) of the iron/polyurethane system. The saturation magnetizations (M_s) of the nanocomposites are 34 and 72 emu/g for the particle loadings of 15 and 40 wt%, corresponding to 213 emu/g and 183 emu/g for the nanoparticles, respectively. M_s in the vinyl ester resin system is much larger than that in the polyurethane system, which is due to the particle oxidation in the polyurethane nanocomposite fabrication process and particle-polymer surface interaction effects.²⁶ The observed smaller H_c after the heat-treatment is due to the decreased interparticle distance concomitant with a stronger dipolar interparticle interaction.

No electric conductivity is detected in the robust vinyl ester resin nanocomposites reinforced with the iron nanoparticles, even at 40 wt% loading, indicating the particle loading is still lower than the percolation threshold. The conductivity improves considerably after the heat treatment. Figure 4 shows the temperature dependent resistivity of the vinyl ester resin nanocomposites after heat treatment at 450 °C for 2 hours. The resistivity increases significantly with decreasing temperature, characteristic of a non-metallic behavior. In view of the high conductivity of iron, the high resistance observed in the 450 °C heat treated specimen is due to the poor conductivity of the carbon matrix. With decreasing temperature, the resistivity increases much faster in the heat-treated 15 wt% nanocomposites than in the heat-treated 40 wt% nanocomposites. This is obviously attributed to the dominating less-conductive carbon matrix in the 15 wt% nanocomposites, as compared to the dominating more-conductive iron in 40 wt% nanocomposites. The observed linear relationship between the logarithmic resistivity and the square root of

temperature $T^{-1/2}$ shown in Figure 4 indicates an interparticle tunneling/hopping conduction mechanism,²⁷ which is different from the observed metallic conduction as observed in the granular Co-Au core-shell nanoparticles.²⁵ The decreased carbon content in the nanocomposite with an initial particle loading of 40 wt% favors electron spin hopping from one particle to another, thus it has a lower resistivity as compared to that of the nanocomposites with an initial particle loading of 15 wt%.

The particle loading was observed to have a dramatic effect on the MR performance of the annealed nanocomposites as shown in Figure 5. A room temperature MR of 8.3 % is observed in the heat-treated nanocomposite with an initial particle loading of 15 wt%. Whereas the heat-treated nanocomposites with an initial particle loading of 20 and 40 wt% show a room-temperature MR of 6.8% and 6.0%, respectively. All of these GMR values are observed at a fairly high field of 90 kOe. Compared to multilayered GMR materials, a high magnetic field is required to saturate the MR, which is characteristic of the tunneling conduction mechanism. However, a 2.0% MR observed at 4.5 kOe still indicates that the GMR in these nanocomposites could be used for biological targeting applications.²⁸ The particle loading dependent MR is attributed to the interparticle distance. In addition, the spacer materials (vinyl ester resin and carbonized vinyl ester resin) play a role in the MR property. The observed field-dependent MR hysteresis loops (Figure 5) in the nanocomposite with high particle loadings are also due to the decreased interparticle distance together with a strong interparticle dipolar interaction.

IV. CONCLUSION

We have shown that a granular GMR nanocomposite can be fabricated by heat treatment of the monomer stabilized iron nanoparticles or robust vinyl ester resin nanocomposites reinforced with iron nanoparticles to induce carbonization of the polymer matrix. The GMR properties depend on the matrix and particle loading, i.e, the spacer distance and the materials between the nanoparticles. The final iron/carbonized nanocomposites exhibit a room temperature GMR of 8.3% at 90 kOe and follow a spin-dependent tunneling conduction.

ACKNOWLEDGEMENTS

This work was supported by QuantumSphere Research Grant (QuantumSphere Inc.) and UC-discovery Grant ELE06-10268. DPY kindly acknowledges support from the National Science Foundation under Grant No. DMR 04-49022.

REFERENCES

- 1 Z. Guo, T. Pereira, O. Choi, Y. Wang, and H. T. Hahn, *J. Mater. Chem* **16**, 2800 (2006).
- 2 S. Stankovich, D. A. Dikin, G. H. B. Dommett, K. M. Kohlhaas, E. J. Zimney, E. A. Stach, R. D. Piner, S. T. Nguyen, and R. S. Ruoff, *Nature* **442**, 282 (2006).
- 3 M. Huang, O. Choi, Y. S. Ju, and H. T. Hahn, *Appl. Phys. Lett.* **89**, 023117 (2006).
- 4 Z. Wang, M. Lu, H. L. Li, and X. Y. Guo, *Mater. Chem. Phys.* **100**, 77 (2006).
- 5 Z. Guo, L. L. Henry, V. Palshin, and E. J. Podlaha, *J. Mater. Chem.* **16**, 1772 (2006).
- 6 S. Lee, H. J. Shin, S. M. Yoon, D. K. Yi, J. Y. Choi, and U. Paik, *J. Mater. Chem.* **18**, 1751 (2008).
- 7 Z. Guo, S. Wei, B. Shedd, R. Scaffaro, T. Pereira, and H. T. Hahn, *J. Mater. Chem.* **17**, 806 (2007).
- 8 D. Zhang, J. A. Downing, F. J. Knorr, and J. L. McHale, *J. Phys. Chem. B.* **110**, 21890 (2006)
- 9 P. Sozzani, S. Bracco, A. Comotti, R. Simonutti, P. Valsesia, Y. Sakamoto, and O. Terasaki, *Nat. Mater.* **5**, 545 (2006).
- 10 B. Sareni, L. Krahenbuhl, A. Beroual, and C. Brosseau, *J. Appl. Phys.* **80**, 4560 (1996).

11. C. Brosseau, P. Queffelec, and P. Talbot, *J. Appl. Phys.* **89**, 4532 (2001).
12. J. Liu, M. Itoh, and K.-I. Machida, *Appl. Phys. Lett.* **88**, 062503 (2006).
13. W. J. E. Beek, M. M. Wienk, and R. A. J. Jassen, *Adv. Mater.* **16**, 1009 (2004).
14. H. Koerner, G. Price, N. A. Pearce, M. Alexander, and R. A. Vaia, *Nat. Mater.* **3**, 115 (2004).
15. R. Mohr, K. Kratz, T. Weigel, M. Lucka-Gabor, M. Moneke, and A. Lendlein, *Proc. Natl. Acad. Sci.* **103**, 3540 (2006).
16. M. M. Miller, P. E. Sheehan, R. L. Edelstein, C. R. Tamanaha, L. Zhong, S. Bounnak, L. J. Whitman, and R. J. Colton, *J. Magn. Magn. Mater.* **225**, 138 (2001).
17. A. Moser, K. Takano, D. T. Margulies, M. Albrecht, Y. Sonobe, Y. Ikeda, S. H. Sun, and E. E. Fullerton, *J. Phys. D* **35**, R157 (2002).
18. C. Giebeler, D. J. Adelerhof, A. E. T. Kuiper, J. B. A. van Zon, D. Oelgeschlager, and G. Schulz, *Sens. Actuators A* **91**, 16 (2001).
19. M. N. Baibich, J. M. Broto, A. Fert, F. Nguyen Van Dau, F. Petroff, P. Eitenne, G. Greuzet, A. Friederich, and J. Chazelas, *Phys. Rev. Lett.* **61**, 2472 (1994).
20. C. Sanchez and F. Ribot, *New J. Chem.* **18**, 1007 (1994).
21. X. Zhang and L. C. Simon, *Macromol. Mater. Eng.* **290**, 573 (2005).

- 22 Z. Guo, K. Lei, Y. Li, H. W. Ng, and H. T. Hahn, *Compos. Sci. Technol.* **68**, 1513 (2008)
- 23 Z. Guo, S. Park, H. T. Hahn, S. Wei, M. Moldovan, A. B. Karki, and D. P. Young, *Appl. Phys. Lett.* **90**, 053111 (2007).
- 24 D. Kechrakos and K. N. Trohidou, *Phys. Rev. B* **58**, 12169 (1998).
- 25 Z. Guo, M. Moldovan, D. P. Young, L. L. Henry, and E. J. Podlaha, *Electrochem. Solid State Lett.* **10**, E31 (2007).
- 26 D. Zhang, K. J. Klabunde, C. M. Sorensen, and G. C. Hadjipanayis, *Phys. Rev. B* **58**, 14167 (1998).
- 27 P. Sheng, *Phys. Rev. Lett.* **31**, 44 (1973).
- 28 D. L. Graham, H. A. Ferreira, and P. P. Freitas, *Trends Biotechnol.* **22**, 455 (2004).

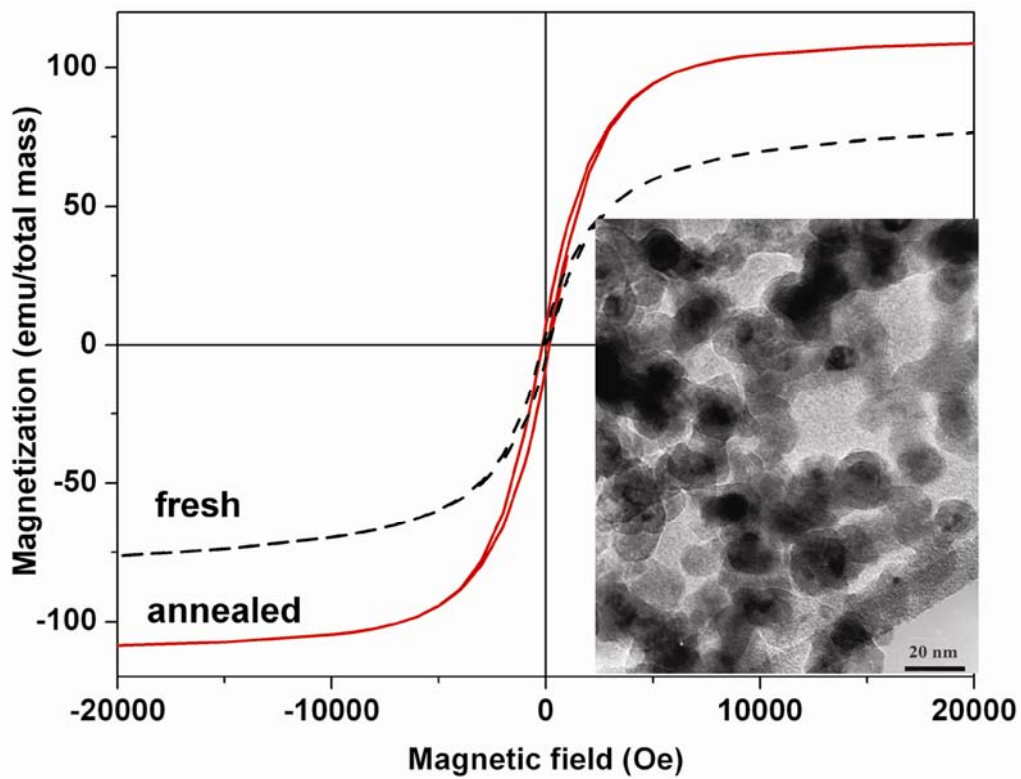


FIG. 1. Magnetic hysteresis loops of the fresh and annealed vinyl ester monomer stabilized iron nanoparticles; inset shows the TEM micrographs of the as-received nanoparticles.

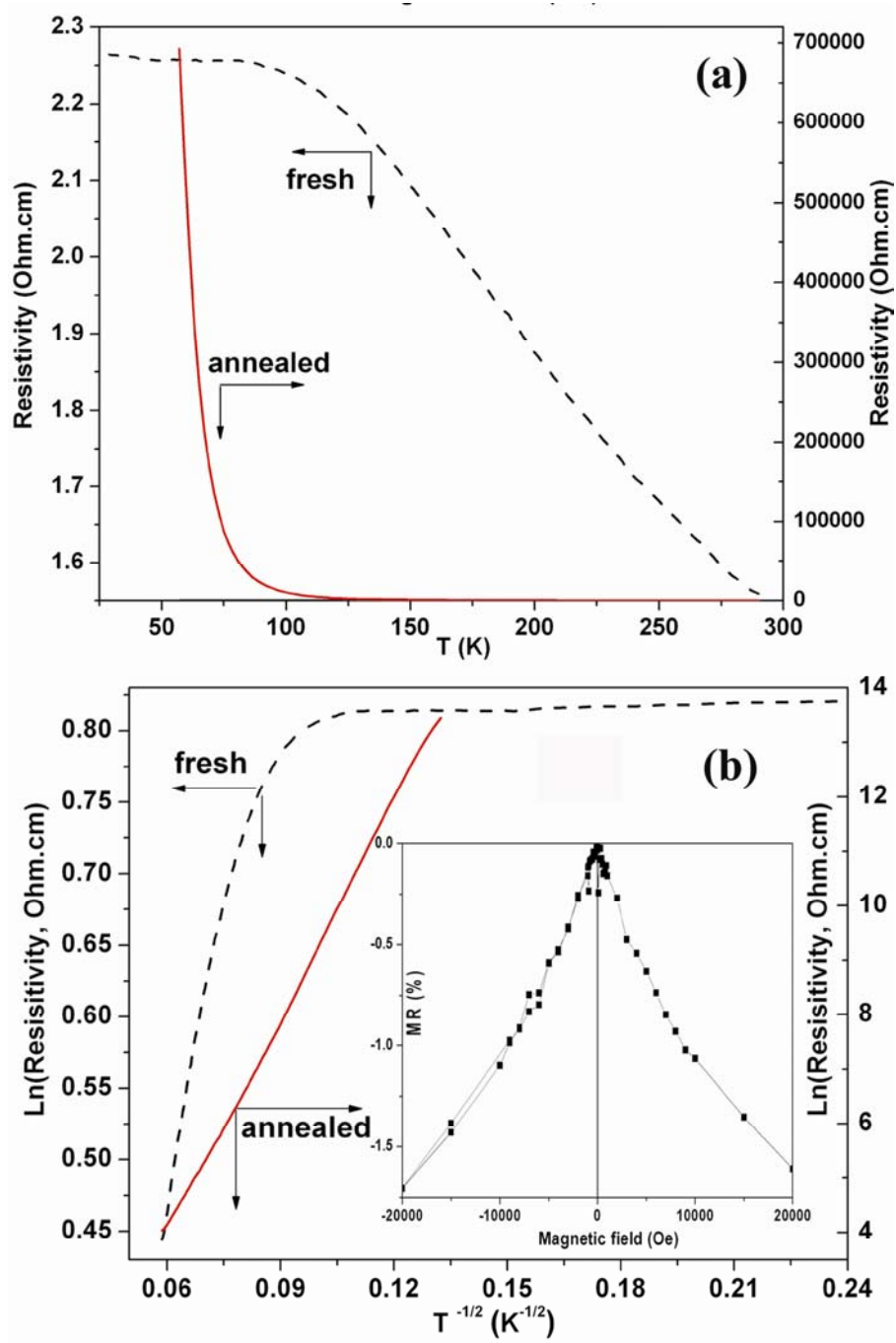


FIG. 2. (a) Temperature dependent resistivity and (b) Ln(resistivity) as a function of $T^{-1/2}$ of as-prepared and heat-treated monomer stabilized iron nanoparticles; inset of (b) shows the MR of the annealed monomer stabilized nanoparticles.

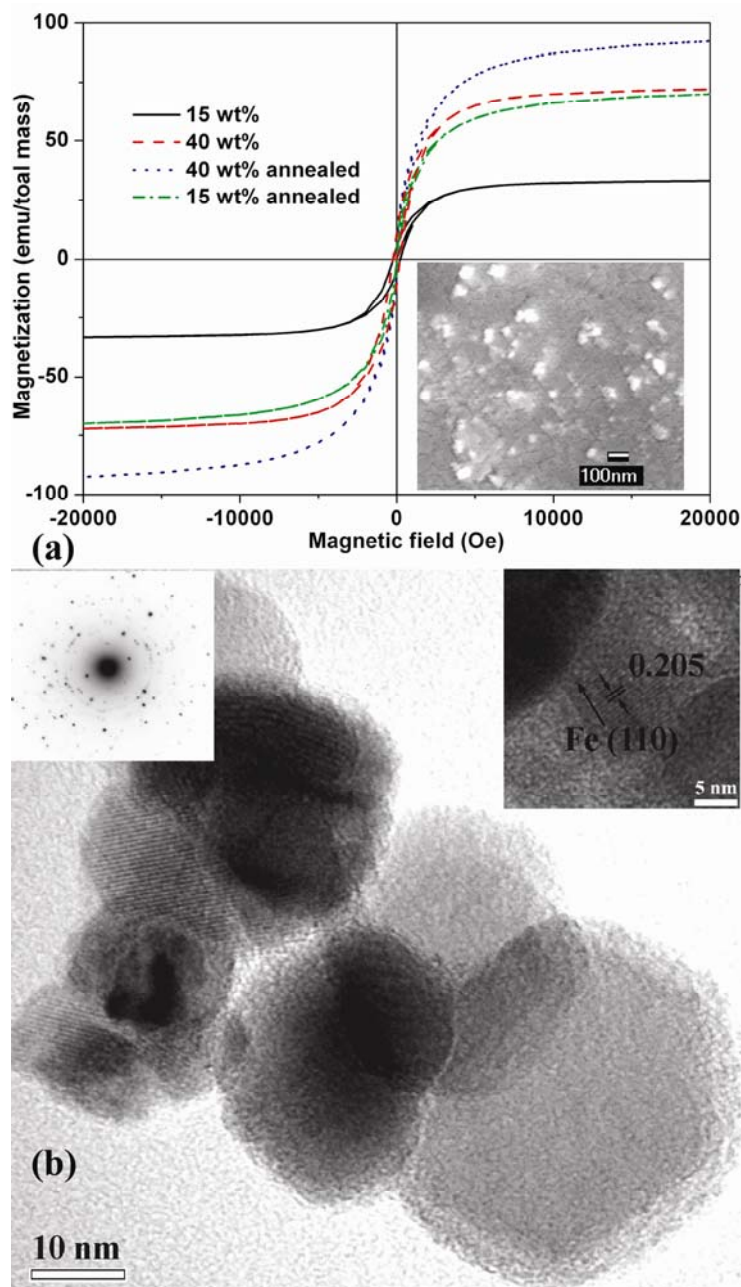


FIG. 3. (a) Hysteresis loops of as-prepared and heat-treated nanocomposites with a particle loading of 15 and 40 wt%, inset shows the SEM image of nanocomposite with a 40 wt% particle loading; and (b) TEM micrograph of the heat-treated nanocomposite, inset shows the SAED and HRTEM images of nanocomposite with a 40 wt% particle loading.

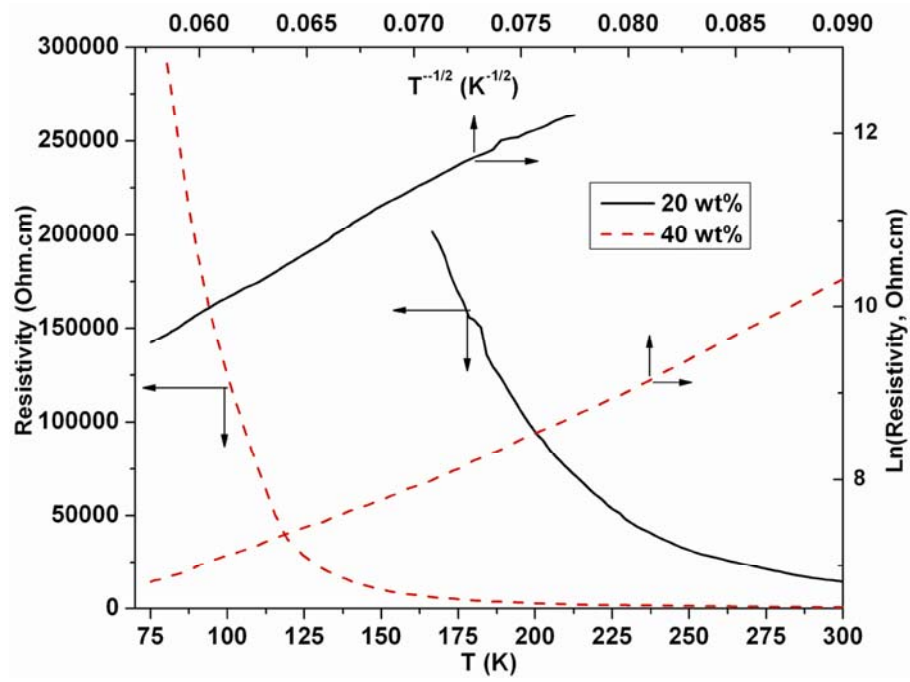


FIG. 4. Temperature dependent resistivity of the nanocomposite with 20 and 40 wt% particle loading after heat treatment at 450 °C.

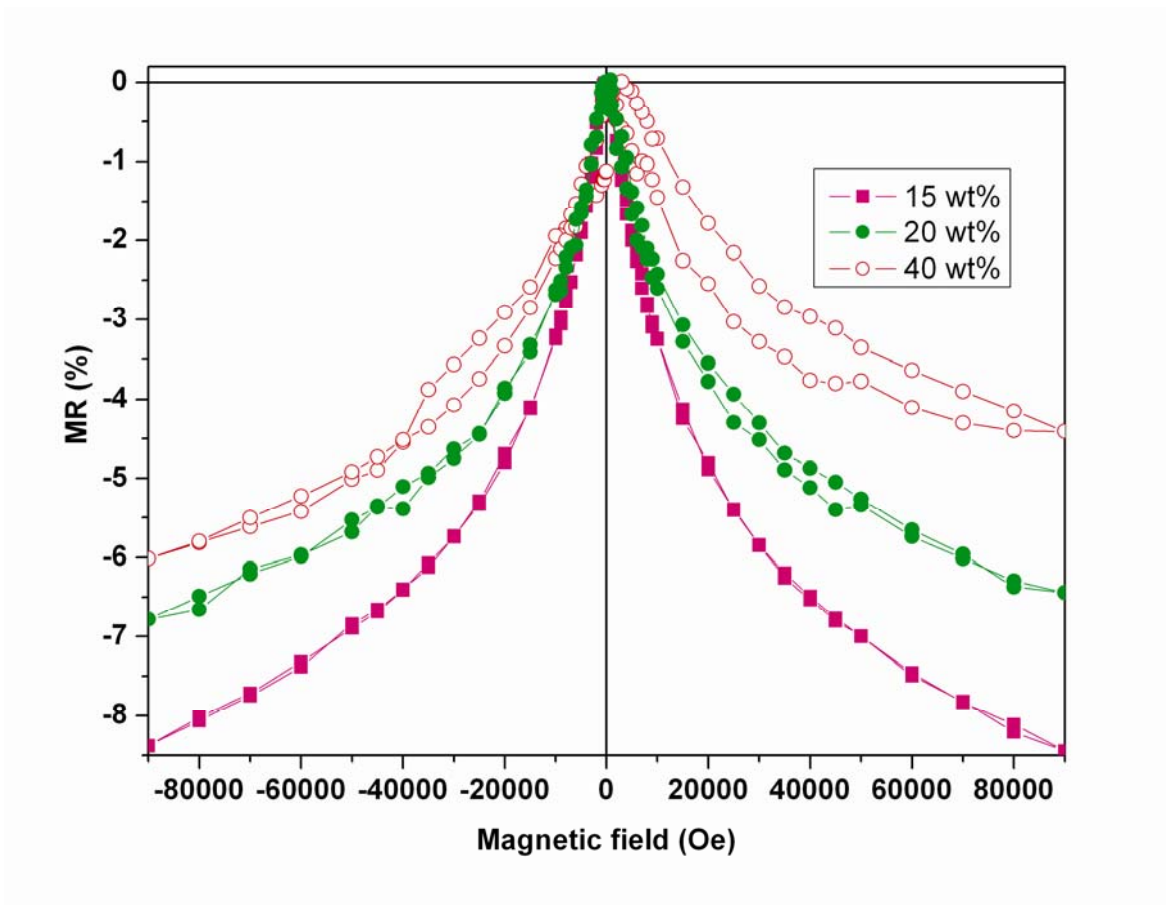


FIG. 5. Room temperature MR as a function of applied field for heat treated nanocomposites reinforced with a particle loading of 15, 20 and 40 wt%, respectively.